

## COMPUTATIONAL STUDY OF UNSTEADY ROAD VEHICLE AERODYNAMICS INCLUDING FLUID-STRUCTURE INTERACTION

Hugo G. Castro<sup>a,b</sup>, Rodrigo R. Paz<sup>b</sup>, Mario A. Storti<sup>b</sup> and Victorio E. Sonzogni<sup>a</sup>

<sup>a</sup>*Grupo de Investigación en Mecánica de Fluidos, Universidad Tecnológica Nacional, Facultad Regional Resistencia, French 414, 3500 Chaco, Argentina, <http://www.frre.utn.edu.ar/gimef>*

<sup>b</sup>*Centro Internacional de Métodos Computacionales en Ingeniería (CIMEC), Instituto de Desarrollo Tecnológico para la Industria Química (INTEC), Universidad Nacional del Litoral - CONICET Güemes 3450, 3000 Santa Fe, Argentina, <http://www.cimec.org.ar>*

**Keywords:** fluid-structure interaction, large eddy simulation, road vehicles, aerodynamics.

**Abstract.** In the study of road vehicle aerodynamics it is often assumed that the vehicle is a rigid body, rigidly attached to the ground. However, that is not the case of real vehicles on the road. They interact with the incident wind, which changes intensity and direction in an unpredictable way and also with bumps and surface imperfections of the road. The interaction between wind and vehicle can be numerically modeled as a fluid-structure interaction (FSI) problem while the road imperfections as a stochastic input force in the system.

However, even at present days, with large computational resources available, experiments are preferred to numerical simulation in the study of vehicle aerodynamics and even in the analysis of FSI problems due to the reliability gained by wind tunnels. Nevertheless, this experimental tool has also shortcomings that can be corrected and even strengths that can be improved by using numerical simulation.

In this work the feasibility of using a computational code to reproduce the experimental conditions in a wind tunnel test section is investigated. This study is focused not only on the aerodynamics of a simplified road vehicle but also on its dynamic interaction with an incident wind flow. The fluid-structure interaction model was tested and the results demonstrated that the computational tools developed in this work enable us to reproduce and/or to assist experimental studies.

## 1 INTRODUCTION

Aerodynamics is the study of a solid body moving through the air and the interaction between the body surface and the surrounding fluid with different relative velocities and directions. Road vehicle aerodynamics adds another source of complexity given the existence of the atmospheric boundary layer (ABL). The wind in the ABL generates a turbulent flow environment, impacting on the mean velocity experienced by the moving vehicle. Furthermore, this turbulence along with the vehicle wake unsteadiness can affect the aerodynamic forces acting on it. If the frequency of these forces matches the natural frequency of the body, it can induce noise and vibrations which could seriously affect the comfort of the driver. The complexity associated with time-varying flows determines that the majority of the investigations have been limited to the time-averaged behaviour.

Computational Fluid Dynamics (CFD) enable us to perform studies on road vehicle aerodynamics by means of the numerical simulation of the governing equations of the physical system. Owing to the large range of lengths and time scales involved in the problems mentioned above, it is generally required a high degree of refinement in the finite element (or finite volume) mesh, resulting in a very large computational resource requirement. Furthermore, in fluid-structure interaction (FSI) problems, fluid and structure dynamics influence each other: the structure deforms under the effect of the fluid forces and the fluid follows the structure displacement. This interaction means not only that the fluid velocity equals that of the structure at the interface, but that the fluid domain changes as a consequence of the motion of the structure. Newer technologies and faster and powerful (super-)computers make now possible to numerically solve this kind of complex problems.

However, the experimental simulation is still preferred to the numerical simulation in the study of vehicle aerodynamics and even in the analysis of fluid-structure interaction problems due to the reliability gained by wind tunnels. This observation is based on the fact that wind tunnels enable the *measurement*, not the *estimation* of the aerodynamic forces, provided that the physics of the fluid flow in the wind tunnel is correct. Also, wind tunnel results have shown a notable agreement with road tests and is a fast, cost-effective and reliable tool (Cooper, 2004). On the other hand, CFD provides the possibility to execute the following tasks:

- i) to perform a detailed analysis of the problem, isolating any aspect of the body geometry if required,
- ii) to further understand the physics of the problem, by means of powerful visualization tools,
- iii) to modify the test conditions in a time and cost efficient manner.

All these characteristics suggest that, if CFD simulations are used to complement experimental test results, then the development cycle of road vehicles can be accelerated.

The aim of this work is to demonstrate that the computational codes developed by the authors can be used to reproduce the experimental conditions in a wind tunnel test section. This study is focused not only on the aerodynamics of a fixed body but also on its dynamic interaction with an incident wind flow.

## 2 ROAD VEHICLE AERODYNAMICS

Understanding ground vehicles aerodynamics allows us to optimize the operation of a wide spectrum of road vehicles, that ranges from passenger (cars, buses, trains) to comercial (trucks

and trains) vehicles. Road vehicle aerodynamics is a complex topic due to the interaction between the air flow and the ground.

Besides of fuel consumption, aerodynamics is directly related to vehicle stability: the flow-vehicle interaction impacts on the straight line stability (roadholding), dynamic passive steering and the response to crosswind. Furthermore, there are other issues where the aerodynamics plays an important role: the accumulation of droplets of rain water on windows and outside mirrors, the accumulation of dirt in headlights, wind noise, etc. In summary, aerodynamics has a significant impact on the design of a vehicle and requires a detailed analysis of the flow around it, including unsteady and turbulent flow phenomena (Hucho, 1998).

A road vehicle has also aerodynamic properties that are specific to this kind of vehicles. Due to its geometry, it can be considered a *bluff body*, which means that drag is mainly due to the pressure acting on it. Skin friction, caused by viscous shear forces on the surface of the vehicle, has only a small contribution to the drag. Flow separation occurs in the back of the body, creating large recirculation regions in the near wake, resulting in a lower pressure on the back surfaces, see figure (1).

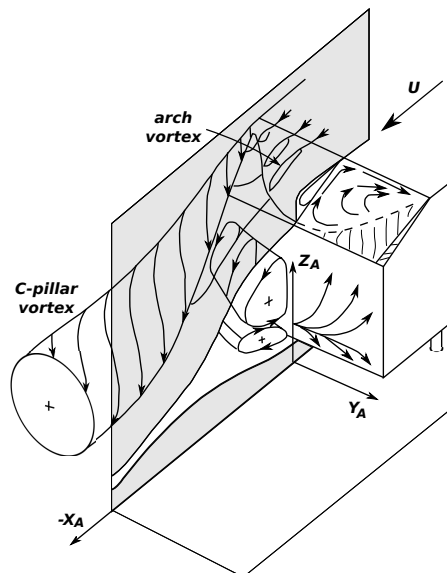


Figure 1: Vortex system behind a road vehicle (Ahmed et al., 1984).

This mechanism produce an increase in the difference between the pressure acting on the front and on the back of the vehicle. According to Wood (2004), approximately the 75 % of the total drag of a light ground vehicle is due to the pressure drag, while for heavy ground vehicles around the 90 % of the drag is pressure drag.

The flow around three-dimensional bluff bodies is characterized by separated shear layers formed at the top, bottom and side edges of the body (Gürlek, 2008). The wake is often dominated by streamwise vortices (which may interact with each other) and its unsteady nature can affect the aerodynamic forces acting on the body.

Until a few years ago, complex aerodynamic studies on road vehicles were performed almost exclusively in wind tunnel facilities. Even today, they still are more frequently used than numerical studies. Nevertheless, CFD nowadays allows predicting unsteady aerodynamic effects due to the improvement of computational power and efficiency. RANS approach was widely used in vehicle aerodynamics studies (Basara et al., 2001; Guilmineau, 2008), however,

unlike the steady-state solution that RANS method can provide, the numerical simulation of unsteady aerodynamic problems requires the use of the LES technique. For example, according to [Guilmineau \(2008\)](#), RANS simulations does not accurately predict the flow pattern around the Ahmed body for a slant angle of  $25^\circ$  while for an angle of  $30^\circ$  this approach worked well. This is because RANS simulations strongly depend on the implemented turbulence model and geometric characteristics of the problem. On the other hand, the use of LES on this particular test case enabled the prediction of the location at which the flow separates from the model as well as the flow structure on the wake ([Krajnovic and Davison, 2004](#)).

As real vehicles have complex geometries, numerical simulations are often carried out with simplified (generic) vehicle geometries. Although many different types of simplified vehicle geometries were proposed, one of the most used is the so called Ahmed model ([Ahmed et al., 1984](#)). This model is considered a standard benchmark and several investigations have been devoted to implement numerical and experimental studies of the flow around this particular model (e.g. [Krajnovic and Davison \(2005\)](#), [Hinterberger et al. \(2004\)](#), [Serre et al. \(2011\)](#)).

Another aspect of the automotive aerodynamics that is rarely explored in the literature is the interaction between an elastically mounted road vehicle model and the airflow. [Cheng et al. \(2011\)](#) investigated the stability characteristics of road vehicles under pitching oscillation. By imposing sinusoidal-forced-pitching oscillation on a sedan-type vehicle model during the LES, the authors found that the front-pillar vortex is the main factor that imparts the unstable tendency on the pitching behaviour of the vehicle. In line with this research, the same authors proposed a dimensionless coefficient that reflects the pitching stability of a vehicle in another paper ([Cheng et al., 2012](#)).

As it was pointed out by [Krajnovic et al. \(2011\)](#), forces and moments obtained in tests where dynamic flow conditions were used, have shown to be different from those found in steady flow conditions. A common approach is to evaluate the aerodynamic performance using static conditions, where the position of the model is changed discontinuously. This approach is known as “quasi-steady” and it is widely employed in experimental tests and numerical simulations.

### 3 AHMED BODY

The Ahmed body is a simplified road vehicle model defined by [Ahmed et al. \(1984\)](#), see figure (2). A more detailed description of the model can be found in the work of [Franck \(2004\)](#); [Franck et al. \(2009\)](#) and references therein.

In the test performed by [Ahmed et al. \(1984\)](#), the model was fixed on cylindrical stilts, 50 mm above a ground board, in an open tunnel test section. A wind speed of 60 m/s was used, corresponding to a model length based Reynolds number of  $4.29 \times 10^6$  and a turbulence intensity less than 0.5%. The authors found that the major contribution to the pressure drag comes from the slant and vertical base surface of rear end. However, several investigations were made with a smaller Reynolds number, a desired feature when LES is considered. [Hinterberger et al. \(2004\)](#) performed LES of the flow over the Ahmed body with a Reynolds number of  $2.88 \times 10^6$  leading to a bulk velocity of 40 m/s while [Krajnovic and Davison \(2004\)](#) used an even smaller velocity of approximately 10 m/s. Interestingly, in this later work the authors have found that the level of the Reynolds number has small influence on the results in highly separated flows around cars provided that it is high enough.

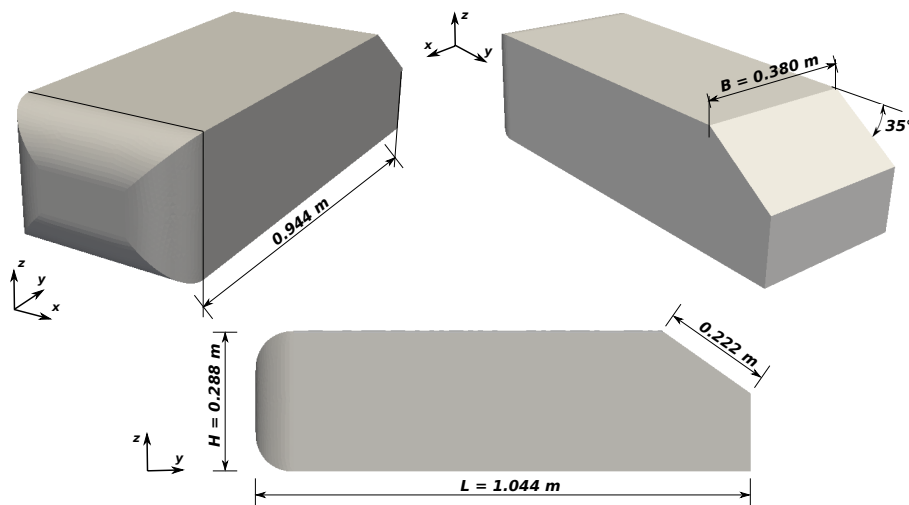


Figure 2: Main dimensions of the simplified model proposed by Ahmed et al. (1984).

### 3.1 Computational domain and inlet boundary conditions

The computational domain was adjusted to the main dimensions of the “Jacek Gorecki” boundary layer wind tunnel in order to provide data for a later comparison with an experimental test. The “Jacek Gorecki” is an open circuit wind tunnel located at the Northeast National University at Resistencia (Chaco), Argentina, which has a 2.4 m wide  $\times$  1.8 m high  $\times$  22.4 m long working section (Wittwer and Möller, 2000). As can be seen in figure (3), the computational domain has a width  $W = 2.40$  m with a height  $H = 1.80$  m and 6.264 m of length. The center of the coordinate system was placed at the inlet plane ( $x = 0$  is the symmetry plane,  $y = 0$  is the inlet plane,  $z = 0$  is the ground plane). No advantage was taken of the symmetry of the problem in order to perceive any asymmetry in the solution.

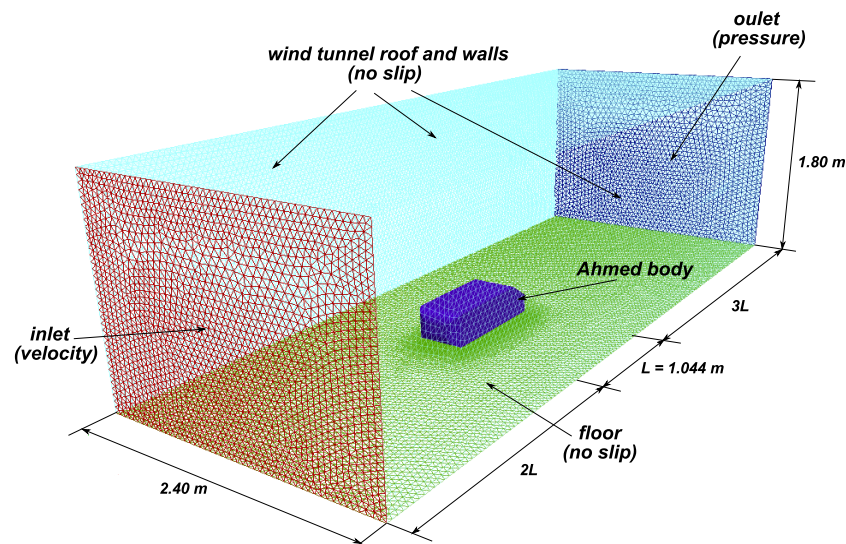


Figure 3: Computational domain of the Ahmed test case.

The body was located at  $2L$  downstream ( $y$ -direction) the inlet section and at  $3L$  upstream the outlet boundary to allow full development of the flow downstream the model, totaling an extension of  $6L$ . Also, the model was placed at a height of 0.05 m above the floor. Non-slip

boundary condition was prescribed at ground, roof and tunnel walls, while null pressure was imposed at the outlet wall. With these conditions the blockage ratio was about 2.6%.

The cross section of the domain used in this work is larger than the one used by [Krajnovic and Davison \(2004\)](#) which consisted in a channel of approximately 1.87 m × 1.40 m (width × height). Also, the boundary conditions on the lateral walls and ceiling are different. In their work, [Krajnovic and Davison \(2004\)](#) treated the lateral surfaces and ceiling as slip surfaces using symmetry conditions in order to reproduce the experimental test of [Lienhart and Becker \(2003\)](#) who performed their experiment in a channel with a 3/4 open test section (with floor but without lateral surfaces or ceiling). This 3/4 open section configuration enables the flow across these surfaces while in the numerical simulation of [Krajnovic and Davison \(2004\)](#) and in the present work that is not possible, leading to a different blockage ratio condition.

The boundary condition at the inlet of the domain calls for a fully developed flow with boundary layers on roof, walls and floor, as this is the case in the wind tunnel test section. To achieve this condition, mean velocity profiles and turbulence intensity values were adopted in agreement with the values reported by [Wittwer and Möller \(2000\)](#). Here again, an observation must be made. The maximum velocity value at the center of the wind tunnel test section is about 27 m/s. This leads to a model length based Reynolds number of approximately  $1.91 \times 10^6$  which is less than the values reported in all the above cited references except for the work of [Krajnovic and Davison \(2004\)](#). Nevertheless, even with a smaller velocity they found, at least for the geometry of this simplified road vehicle model, that the external vehicle flow at high Reynolds numbers becomes independent of it.

The turbulent flow inside the wind tunnel evolves spatially, therefore the flow downstream is highly dependent on the inflow conditions. So it is important that the turbulent inflow conditions are represented as realistically as possible. In order to achieve this condition, the MDSRFG method was applied ([Castro and Paz, 2013](#)), which is based on the previous works of [Huang et al. \(2010\)](#); [Smirnov et al. \(2001\)](#). To represent adequately the statistical properties of the turbulent flow velocity field  $\mathbf{u}(\mathbf{x}, t)$ , time and space correlations are introduced strictly in the mathematical formulation of the MDSRFG method:

$$u_i(\mathbf{x}, t) = \sum_{m=1}^M \sum_{n=1}^N \left[ p_i^{m,n} \cos \left( \tilde{k}_j^{m,n} \tilde{x}_j + \omega_{m,n} \frac{t}{\tau_0} \right) + q_i^{m,n} \sin \left( \tilde{k}_j^{m,n} \tilde{x}_j + \omega_{m,n} \frac{t}{\tau_0} \right) \right] \quad (1)$$

where

$$p_i^{m,n} = \text{sign}(r_i^{m,n}) \sqrt{\frac{4C_i}{N} E_i(k_m) \Delta k_m \frac{(r_i^{m,n})^2}{1 + (r_i^{m,n})^2}}, \quad (2)$$

$$q_i^{m,n} = \text{sign}(r_i^{m,n}) \sqrt{\frac{4C_i}{N} E_i(k_m) \Delta k_m \frac{1}{1 + (r_i^{m,n})^2}}. \quad (3)$$

$$\tilde{\mathbf{x}} = \frac{\mathbf{x}}{L_s}, \quad (4)$$

$$\tilde{\mathbf{k}}^{m,n} = \frac{\mathbf{k}^{m,n}}{k_0}, \quad (5)$$

with  $\omega_{m,n} \in N(0, 2\pi f_m)$ ,  $f_m = k_m U_{\text{avg}}$ ,  $a$  is a random number uniformly distributed between

0 and 1,  $\zeta$  and  $\xi$  are the vector form of  $\zeta_i^n$  and  $\xi_i^n$ , which are random numbers selected independently from  $N(0, 1)$ . Here,  $N(\mu, \sigma)$  represents a normal distribution with mean  $\mu$  and standard deviation  $\sigma$ . In equations (4) and (5)  $L_s$  is a scale factor related to the length scale of turbulence and  $k_0$  is the lowest wavenumber of the discrete spectrum. Furthermore,  $r_i^{m,n}$  is a random number, independently selected from a three dimensional Normal distribution with zero mean ( $\mu_r = 0$ ) and rms value of one ( $\sigma_r = 1$ ) and  $c_i$  is a function value that depends on the form of the spectrum. More details about the analytical derivation and implementation of the MDSRFG method can be found in the work of [Castro and Paz \(2013\)](#).

### 3.2 Mesh details

The grid used for this test case has 462,580 nodes, 2,192,778 elements and  $h = 0.001$  m, being  $h$  the mean thickness of the first element layer (measured from the model surface). The grid was refined close to the body surface in order to account for viscous effects at the wall and to adequately capture the changes in flow variables within the boundary layer region. An unstructured mesh consisting of tetrahedral and prismatic (wedges) finite elements was used for these tests and was divided in three different regions to account for the mesh movement, figure (4).

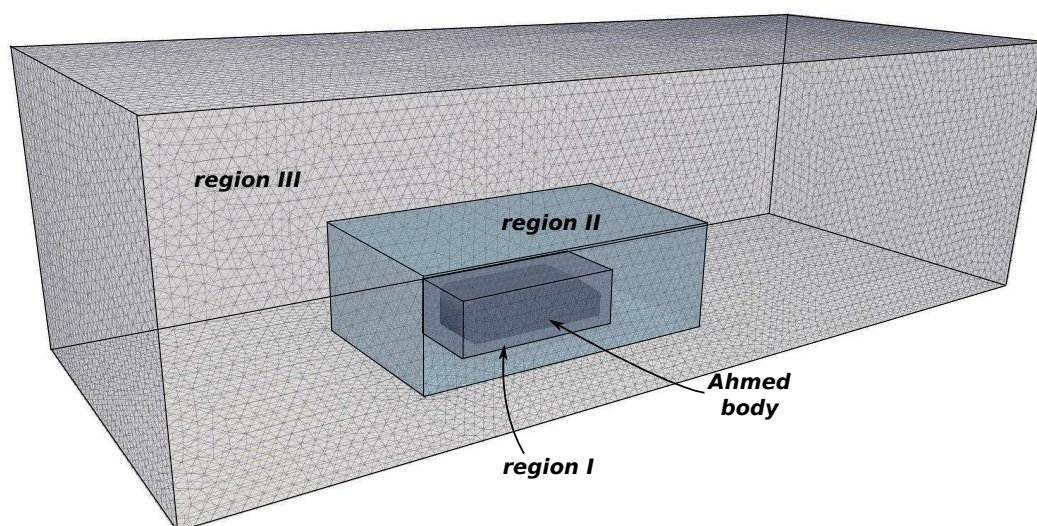


Figure 4: Different regions of the mesh.

## 4 RESULTS AND DISCUSSION

An incompressible Newtonian viscous fluid model is adopted with kinematic viscosity  $\mu = 1.45 \times 10^{-5}$  m<sup>2</sup>/s and density  $\rho = 1.225$  kg/m<sup>3</sup>. The simulations were performed with the PETSc-FEM code (<http://www.cimec.org.ar/petscfem>) using the Finite Element Method to solve the momentum and continuity equations for the velocity and pressure at each node and at each time step ([Storti et al., 2002](#)). The SUPG/PSPG discretization scheme of the incompressible Navier-Stokes equations are implemented ([Brooks and Hughes, 1982](#); [Hughes and Brooks, 1979](#)).

The simulations were performed using two different Beowulf kind of clusters. The “Aquilaes” cluster, with 80 nodes Pentium 4 CPU 3.00 GHz and a server Xeon E5335 2.00 GHz, interconnected via a Gigabit Ethernet network, and the “Coyote” cluster, with 7 nodes Xeon E5420 2.50

GHz (2 x 4 cores), 16 nodes Xeon W3690 3.47 GHz (1 x 6 cores) and a server Xeon E5335 2.00 GHz (2 x 4 cores).

#### 4.1 Static model simulation

The time history of the aerodynamic forces and moments in all three directions, i.e., side ( $F_x$ ), drag ( $F_y$ ) and lift ( $F_z$ ) forces (figure (5)) and pitch ( $M_x$ ), roll ( $M_y$ ) and yaw ( $M_z$ ) moments (figure (6)) were computed during the simulation by adding the viscous and pressure forces around the full three-dimensional model. The deviation (rms values) of the drag force was found to be around 1.3% of the mean value. The corresponding force coefficients were also computed as:

$$C_S = \frac{F_x}{\frac{1}{2}\rho U_\infty^2 A} \quad C_D = \frac{F_y}{\frac{1}{2}\rho U_\infty^2 A} \quad C_L = \frac{F_z}{\frac{1}{2}\rho U_\infty^2 A} \quad (6)$$

being  $C_S$ ,  $C_D$  and  $C_L$  the side, drag and lift force coefficients, respectively, and  $A$  the frontal area of the vehicle model. Mean and rms values of these coefficients are presented in table (1-a)).

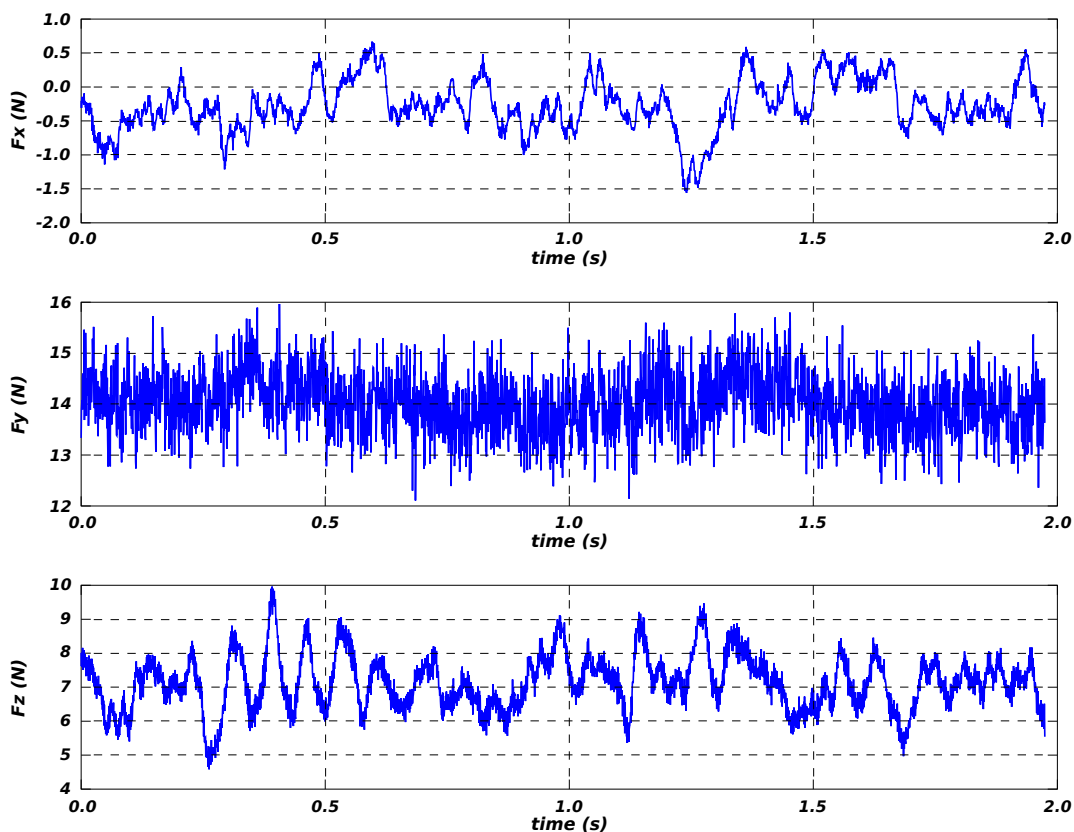


Figure 5: Time history of the aerodynamic forces.

	(a)			(b)		
	$C_S$	$C_D$	$C_L$	$C_S$	$C_D$	$C_L$
mean	-0.006	0.297	0.151	-0.001	0.267	0.035
rms	0.008	0.013	0.017	0.010	0.013	0.022

Table 1: Ahmed static test: time-averaged side ( $C_S$ ), drag ( $C_D$ ) and lift ( $C_L$ ) coefficients (mean and rms values). (a) no-slip condition in the tunnel floor, (b) sliding ground.

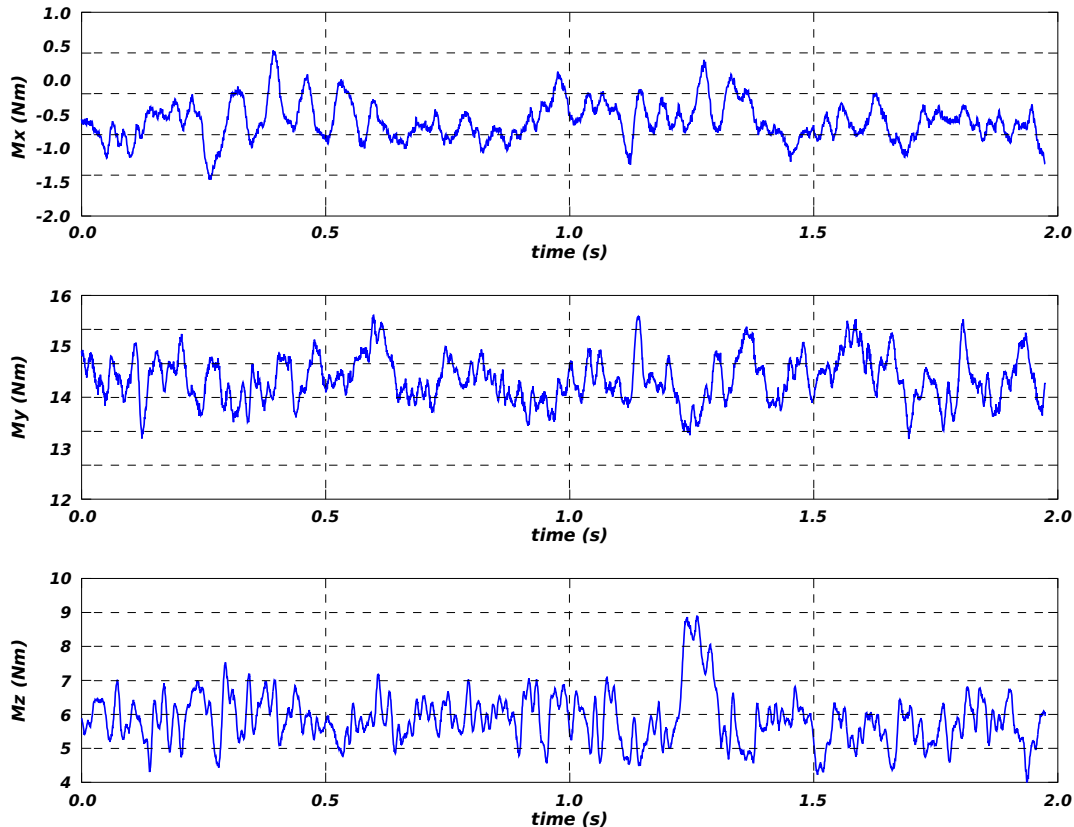


Figure 6: Time history of the aerodynamic moments.

As can be noted, the mean drag force coefficient was found to be higher than the value  $C_{D_{mean}} = 0.255$  obtained by [Ahmed et al. \(1984\)](#). Therefore, another simulation was performed under the same conditions except for the tunnel floor boundary condition, which was modified to simulate a moving ground by imposing the incoming mean velocity  $U_\infty$  as the velocity of the lower wall. This was done in order to validate the numerical model against the experimental study. The results of this later simulation are resumed in table (1-(b)). The mean drag force coefficient still exceeds the value reported by [Ahmed et al. \(1984\)](#) but with a difference less than 5%, highlighting the interference effect that the fixed floor boundary layer causes over the flow pattern and, as a consequence, over the aerodynamic forces.

## 4.2 Fluid-structure interaction study

**Forced vibration.** As a first step prior to the fully coupled fluid-structure interaction study, a test considering an imposed model movement was performed. The main idea behind this test was to verify the correct behaviour of the code in charge of the communication between

the fluid problem and the structure problem. Two degrees of freedom were considered namely lateral movement and yawing, see figure (7). The geometric properties of the Ahmed body (assuming unitary constant density) are listed in table (2), where  $x_o$ ,  $y_o$  and  $z_o$  are the distance of the local coordinate center from the front of the model and  $I_x$ ,  $I_y$  and  $I_z$  are the moments of inertia about the local axes.

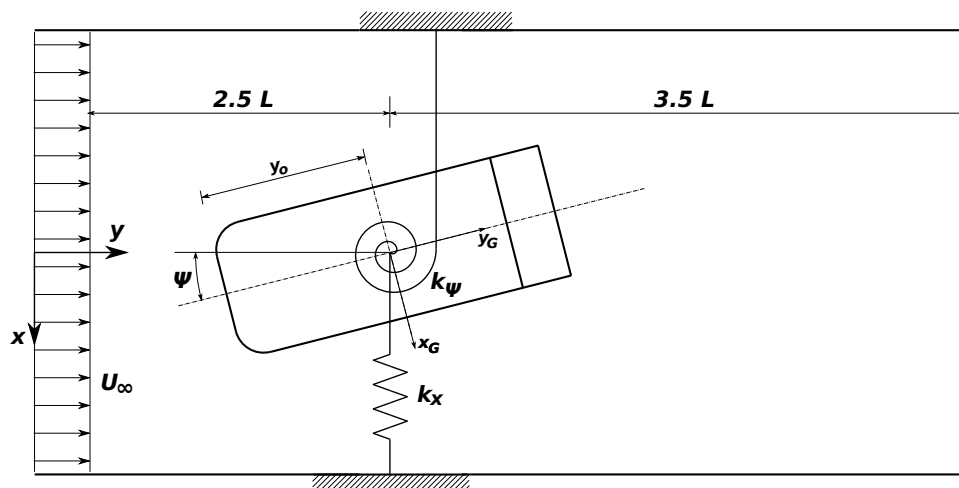


Figure 7: Mechanical configuration of the Ahmed body (top view).

A forced-sinusoidal-yawing ( $M_z$ ) and a forced-sinusoidal-lateral ( $F_x$ ) oscillation were imposed on the vehicle model:

$$\begin{aligned} F_x &= P_o \sin(\omega_F t) \\ M_z &= M_o \sin(\omega_M t) \end{aligned} \quad (7)$$

where  $\omega_F$  and  $\omega_M$  are the loading frequency of the lateral force and yawing moment, respectively. With these settings, the following system of ordinary differential equations is obtained:

$$\begin{aligned} m\ddot{x} + k_x x + d_x \dot{x} &= -F_x(t) \\ I_\psi \ddot{\psi} + k_\psi \psi + d_\psi \dot{\psi} &= M_z(t) \end{aligned} \quad (8)$$

being  $I_\psi \equiv I_z$ ,  $m$  the mass of the model (in case equal to its volume),  $k_x$ ,  $k_\psi$ , the bending and torsional stiffness, respectively, and  $d_x$ ,  $d_\psi$ , the bending and torsional damping, respectively.

Volume (m <sup>3</sup> )	Centroid (m)			Inertia (kg m <sup>2</sup> )		
	$x_o$	$y_o$	$z_o$	$I_x$	$I_y$	$I_z$
0.1099	0.00	0.52	0.14	0.0098	0.0021	0.0104

Table 2: Geometrical data for the Ahmed test case.

Assuming that the system (8) is underdamped, that is,  $0 < \xi_x = d_x/d_x^c < 1$  and  $0 < \xi_\psi = d_\psi/d_\psi^c < 1$ , where  $d_x^c = 2\sqrt{mk_x}$  and  $d_\psi^c = 2\sqrt{I_\psi k_\psi}$  are the critical damping for the motion in the  $x$ -direction and for the yawing motion, respectively, and with the initial conditions

$x(0) = \psi(0) = 0$  and  $\dot{x}(0) = \dot{\psi}(0) = 0$ , then its solution is given by:

$$\begin{aligned} x(t) &= e^{-\xi_x \omega_x t} [A_1 \cos(\omega_D^x t) + B_1 \sin(\omega_D^x t)] + C_1 \cos(\omega_F t) + D_1 \sin(\omega_F t) \\ \psi(t) &= e^{-\xi_\psi \omega_\psi t} [A_2 \cos(\omega_D^\psi t) + B_2 \sin(\omega_D^\psi t)] + C_2 \cos(\omega_M t) + D_2 \sin(\omega_M t) \end{aligned} \quad (9)$$

where

$$\begin{aligned} C_1 &= \frac{P_o}{k_x} \frac{-2\xi_x \frac{\omega_F}{\omega_x}}{\left[1 - \left(\frac{\omega_F}{\omega_x}\right)^2\right]^2 + \left[2\xi_x \left(\frac{\omega_F}{\omega_x}\right)\right]^2} & C_2 &= \frac{M_o}{k_\psi} \frac{-2\xi_\psi \left(\frac{\omega_M}{\omega_\psi}\right)^2}{\left[1 - \left(\frac{\omega_M}{\omega_\psi}\right)^2\right]^2 + \left[2\xi_\psi \left(\frac{\omega_M}{\omega_\psi}\right)\right]^2} \\ D_1 &= \frac{P_o}{k_x} \frac{1 - \left(\frac{\omega_F}{\omega_x}\right)^2}{\left[1 - \left(\frac{\omega_F}{\omega_x}\right)^2\right]^2 + \left[2\xi_x \left(\frac{\omega_F}{\omega_x}\right)\right]^2} & D_2 &= \frac{M_o}{k_\psi} \frac{1 - \left(\frac{\omega_M}{\omega_\psi}\right)^2}{\left[1 - \left(\frac{\omega_M}{\omega_\psi}\right)^2\right]^2 + \left[2\xi_\psi \left(\frac{\omega_M}{\omega_\psi}\right)\right]^2} \end{aligned} \quad (10)$$

and

$$\begin{aligned} A_1 &= -C_1 & A_2 &= -C_2 \\ B_1 &= \frac{C_1 \xi_x \omega_x - D_1 \omega_D^x}{\omega_F} & B_2 &= \frac{C_2 \xi_\psi \omega_\psi - D_2 \omega_D^\psi}{\omega_M} \end{aligned} \quad (11)$$

where  $\omega_x = \sqrt{k_x/m}$  and  $\omega_\psi = \sqrt{k_\psi/I_\psi}$  are the natural frequency of the lateral and yawing oscillation, while  $\omega_D^x = \omega_x \sqrt{1 - \xi_x^2}$  and  $\omega_D^\psi = \omega_\psi \sqrt{1 - \xi_\psi^2}$  are the corresponding damped frequency in each degree of freedom. The structural properties used in this test are listed in table (3).

$P_o$ (N)	$M_o$ (Nm)	$\omega_F$ (rad/s)	$\omega_M$ (rad/s)	$k_x$ (N/m)	$k_\psi$ (Nm/rad)	$d_x$ (Ns/m)	$d_\psi$ (Nms/rad)
170	5	50	50	100	6	13.34	1.00

Table 3: Structural properties for the Ahmed forced oscillation test case.

The lateral displacement and yaw angle for different times in the simulation are shown in figure (8). For the sake of simplicity only 10 time frames are represented here. As it can be seen from figure (8), the algorithm in charge of passing the forces and moments to the structure works well for the case of forced oscillation.

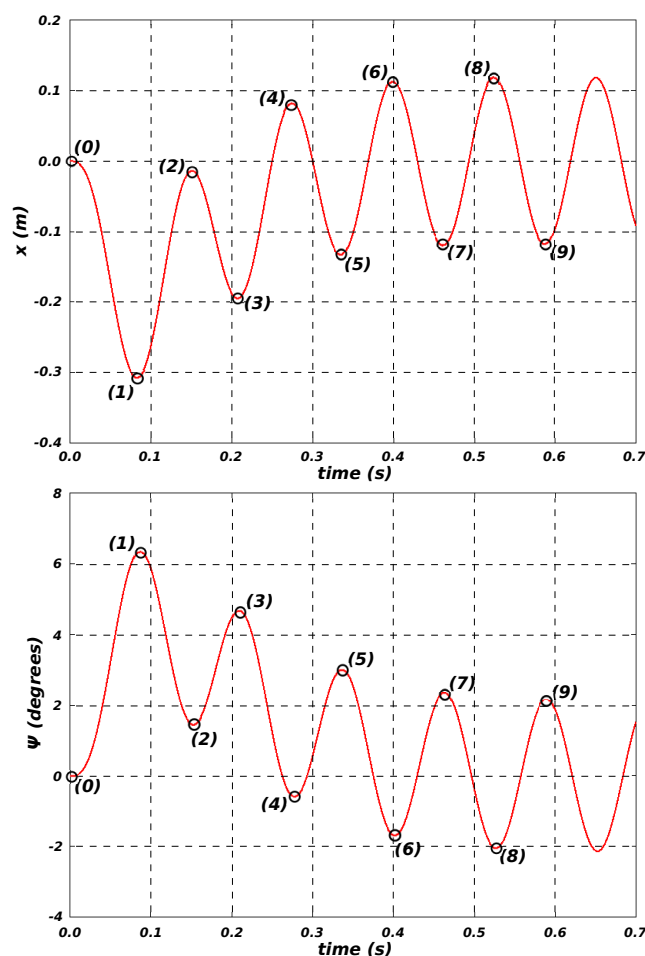


Figure 8: Time history of lateral displacement (top) and yaw angle (bottom). Numerical simulation (circles) and analytic solution (red line).

**Full fluid-structure coupling.** There are, to the authors knowledge, no numerical or experimental FSI studies of simplified road vehicle models. All investigations so far were focused on the forced oscillation of simplified models (Krajnovic et al., 2011; Cheng et al., 2011, 2012; Gilliéron et al., 2003) but none with a full coupling between the fluid and the structure. Therefore, some numerical experiments were performed in order to analyze this phenomenon.

Two simulations with the following parameters were considered:  $m = 0.5495$  kg,  $I_\psi = 0.052$  kgm<sup>2</sup>,  $k_x = 100$  N/m,  $k_\psi = 6$  Nm/rad,  $\rho = 5$  kg/m<sup>3</sup> and were carried out with and without inlet synthesized turbulence. The particular parameters of each simulation are listed in table (4).

	Turbulence synthesis	$d_x$ (Ns/m)	$d_\psi$ (Nms/rad)
test I-a	no	13.343	1.005
test I-b	yes	13.343	1.005

Table 4: Structural properties for the Ahmed FSI test case.

In figures (9) and (10) the lateral and angular displacements of the Ahmed body are shown. For test I-a the minimum/maximum values are  $-0.05$  m/0.23 m (lateral displacement) and

$-15^\circ/28^\circ$  (yawing), while for test I-b are  $-0.16$  m/0.23 (lateral displacement) and  $-25^\circ/8^\circ$  (yawing). The influence of synthesized turbulence is evidenced by the vortex structures visualized with Q isosurfaces.

These results demonstrate that by using the numerical tools presented in this work it is possible to reproduce an experimental test in a wind tunnel. In particular, it is possible to assess experimental FSI studies by a computational model, reproducing all the mechanical and dynamical characteristics of a road vehicle model along with the turbulent flow that interacts with it.

## **5 CONCLUSIONS**

The interaction of a fluid with a structure is an important phenomenon that has to be considered in many engineering applications. Particularly, the interaction between a dynamic vehicle model and the airflow is an aspect of the automotive aerodynamics that is poorly investigated. In this work the study of the aerodynamic characteristics of a simplified road vehicle model under the action of a turbulent air flow was performed with the aim of simulating a wind tunnel test.

A simplified model known as the Ahmed body was studied under two different scenarios: considering the model as a rigid one and by assigning it dynamic properties. The fluid-structure interaction model was tested and the results demonstrated that the computational tools developed in this work enable us to reproduce and/or assist experimental studies.

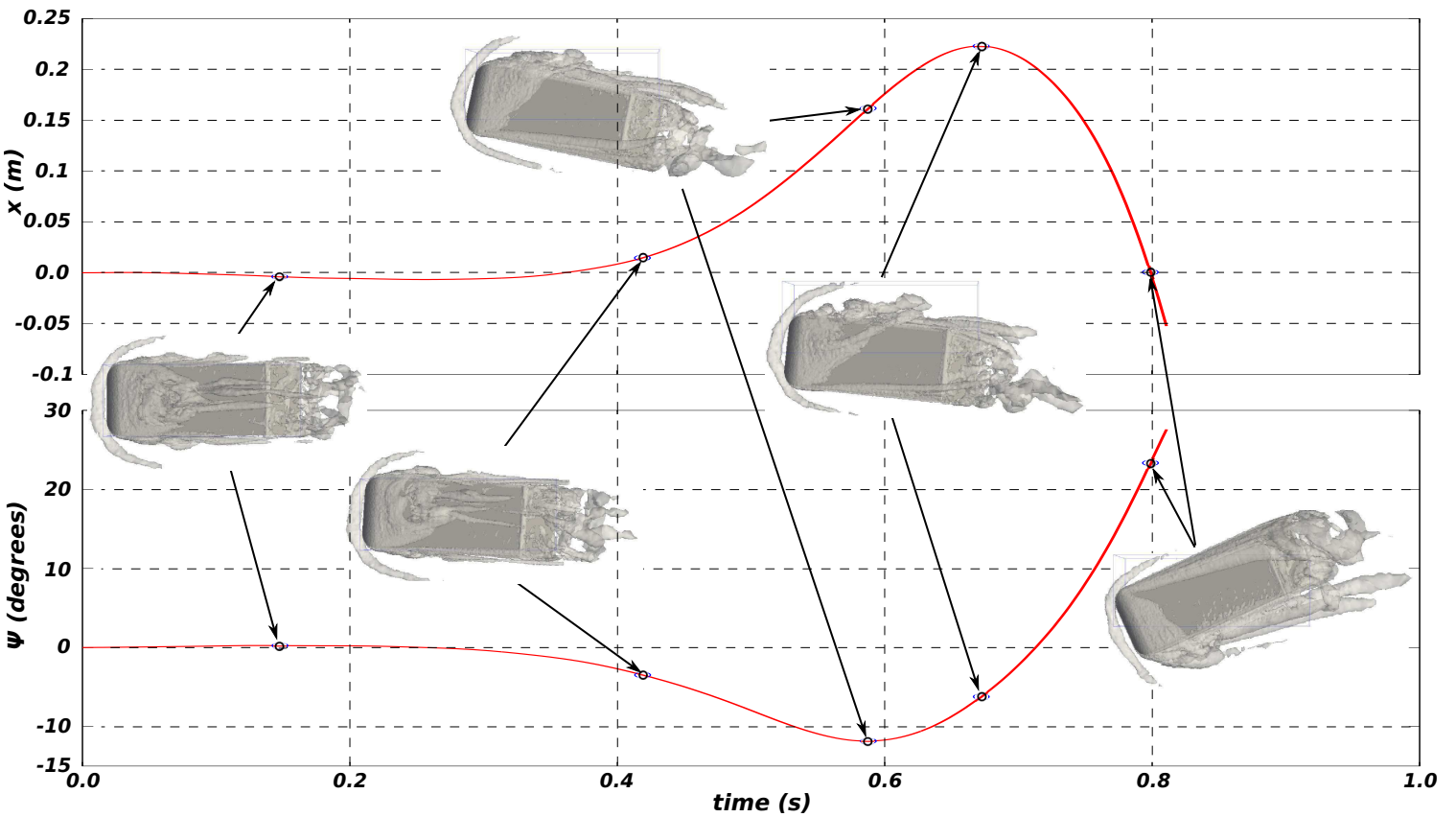
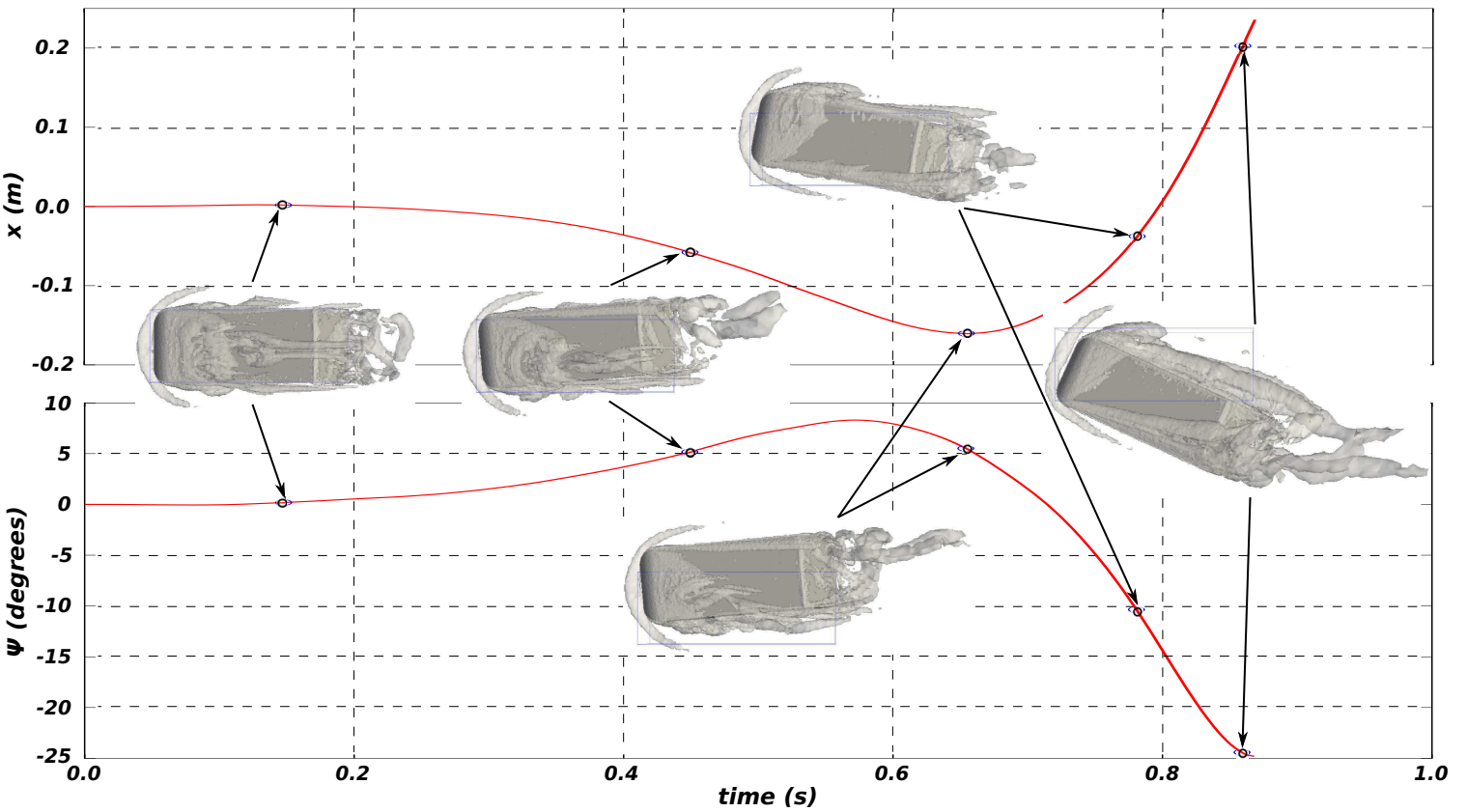


Figure 10. Results of the coupled FSI test I-a. The red line indicates lateral displacement (top) and yaw angle (bottom). Also, the geometric configuration of the Ahmed body at different instants is shown (top view).



Ahmed FSI test I-b. The red line indicates lateral displacement (top) and yaw angle (bottom). Also, the geometric configuration of the Ahmed body at different instants is shown (top view).

## REFERENCES

- Ahmed S.R., Ramm G., and Faltin G. Some salient features of the times-averaged ground vehicle wake. *Society of Automotive Eng., Inc*, 1:1–31, 1984.
- Basara B., Przulj V., and Tibaut P. On the calculation of external aerodynamics industrial benchmarks. *SAE paper*, 2001-01-0701, 2001.
- Brooks A. and Hughes T. Streamline upwind/Petrov-Galerkin formulations for convection dominated flows with particular emphasis on the incompressible Navier-Stokes equations. *Computational Methods in Applied Mechanics and Engineering*, 32:199–259, 1982.
- Castro H. and Paz R. A time and space correlated turbulence synthesis method for large eddy simulations. *Journal of Computational Physics*, 235:742–763, 2013.
- Cheng S., Tsubokura M., Nakashima T., Nouzawa T., and Okada Y. A numerical analysis of transient flow past road vehicles subjected to pitching oscillation. *Journal of Wind Engineering and Industrial Aerodynamics*, 98:511–522, 2011.
- Cheng S., Tsubokura M., Nakashima T., Okada Y., and Nouzawa T. Numerical quantification of aerodynamic damping on pitching vehicle-inspired bluff body. *Journal of Fluids and Structures*, 30:188–204, 2012.
- Cooper K. Commercial vehicle aerodynamic drag reduction: historical perspective as a guide. In *Aerodynamics of Heavy Vehicle: Trucks, Buses and Trains*, pages 9–28. Springer, 2004.
- Franck G. *Aerodinámica de vehículos mediante una resolución de las ecuaciones de Navier-Stokes con cálculo distribuido*. Master's Thesis, Facultad de Ingeniería Química, Universidad Nacional del Litoral, 2004.
- Franck G., Nigro N., Storti M., and D'Elía J. Numerical simulation of the flow around the ahmed vehicle model. *Latin American Applied Research*, 39:295–306, 2009.
- Gilliéron P., Chometon F., and Laurent J. Analysis of hysteresis and phase shifting phenomena in unsteady three-dimensional wakes. *Experiments in Fluids*, 35:117–129, 2003.
- Guilmineau E. Computational study of flow around a simplified car body. *Journal of Wind Engineering and Industrial Aerodynamics*, 96(6-7):1207 – 1217, 2008. ISSN 0167-6105. doi:DOI:10.1016/j.jweia.2007.06.041. 5th International Colloquium on Bluff Body Aerodynamics and Applications.
- Gürlek C. *Study of the flow around a bus model*. Ph.D. thesis, Dept. of Mechanical Engineering, Çukurova University, 2008.
- Hinterberger C., García-Villalba M., and Rodi W. Large eddy simulation of flow around the Ahmed body. *Lectures Notes in Applied and Computational Mechanics, The Aerodynamics of Heavy Vehicles: Trucks, Buses and Trains*, McCallen, F. Browand, J. Ross (Eds.), Springer Verlag, 2004.
- Huang S., Li Q., and Wu J. A general inflow turbulence generator for large eddy simulation. *Journal of Wind Engineering and Industrial Aerodynamics*, 98:600–617, 2010.
- Hucho W. *Aerodynamics of road vehicles*. SAE Publishing, 1998.
- Hughes T. and Brooks A. A multi-dimensional upwind scheme with no crosswind diffusion. In *Finite Element Methods for Convection Dominated Flows*, ASME ed., 34:19–35, 1979.
- Krajnovic S., Bengtsson A., and Basara B. Large eddy simulation investigation of the hysteresis effects in the flow around an oscillating ground vehicle. *Journal of Fluids Engineering*, 133, 121103, 2011.
- Krajnovic S. and Davison L. Large eddy simulation of the flow around a simplified car model. In *2004 SAE World Congress*, volume SAE Paper 2004-01-0227. Detroit, Michigan, USA, 2004.

- Krajnovic S. and Davison L. Flow around a simplified car, Part 1: Large Eddy Simulation. *Journal of Fluids Engineering*, 127:907–918, 2005.
- Lienhart H. and Becker S. Flow and turbulence structure in the wake of a simplified car model. *SAE paper*, 2003-01-0656, 2003.
- Serre E., Minguez M., Pasquetti R., Guilmineau E., Bo Deng G., Kornhaas M., Schäfer M., Fröhlich J., Hinterberger C., and Rodi W. On simulating the turbulent flow around the Ahmed body: A French-German collaborative evaluation of LES and DES. *Computers & Fluids*, In press, 2011. doi:DOI:10.1016/j.compfluid.2011.05.017.
- Smirnov A., Shi S., and Celik I. Random flow generation technique for large eddy simulations and particle-dynamics modeling. *Journal of Fluids Engineering*, 123:359–371, 2001.
- Storti M., Nigro N., Paz R., and Dalcín L. PETSc-FEM: A general purpose, parallel, multi-physics FEM program. 2002.
- Wittwer A. and Möller S. Characteristics of the low speed wind tunnel of the UNNE. *Journal of Wind Engineering and Industrial Aerodynamics*, 84:307–320, 2000.
- Wood R. Impact of advanced aerodynamic technology on transportation energy consumption. *SAE paper*, 2004-01-1306, 2004.